LA-UR-19-20825 (Accepted Manuscript)

Highly Ordered N-Doped Carbon Dots Photosensitizer on Metal–Organic Framework-Decorated ZnO Nanotubes for Improved Photoelectrochemical Water Splitting

Han, Hyungkyu

To be published in: Small

DOI to publisher's version: 10.1002/smll.201902771

Permalink to record: http://permalink.lanl.gov/object/view?what=info:lanl-repo/lareport/LA-UR-19-20825

Highly Ordered N-Doped Carbon Dots Photosensitizer on Metal-Organic Framework-decorated ZnO Nanotubes for Improved Photoelectrochemical Water Splitting

Hyungkyu Han[1*], Frantisek Karlicky[2], Sudhagar Pitchaimuthu[3], Sun Hae Ra Shin[4], Aiping Chen[1]

[1] Center for Integrated Nanotechnologies, Los Alamos National Laboratory, Los Alamos, NM 87545, USA

[2] Department of Physics, Faculty of Science, University of Ostrava, 30. Dubna 22, 701 03 Ostrava, Czech

[3] Multi-funcional Photocatalyst and Coatings Group, SPECIFIC, College of Engineering, Swansea University, Swansea SA1 8EN, Wales, United Kingdom

[4] Center for Integrated Nanotechnologies, Sandia National Laboratories, Albuquerque, NM 87185, USA

RECEIVED DATE (to be automatically inserted after your manuscript is accepted if required according to the journal that you are submitting your paper to)

Corresponding Author*

Hyungkyu Han (hhan@lanl.gov)

Abstract

In spite of having several advantages such as low cost, high chemical stability, and environmentally safe and benign synthetic as well as operational procedures, the full potential of carbon dots (CDs) are yet to be explored as photosensitizers due to the challenges associated with the fabrication of well-arrayed CDs with any other photocatalytic heterostructures. In the present study, a unique combination of Metal-organic frameworks (MOFs) decorated Zinc Oxide (ZnO) one-dimensional (1D) nanostructures as host and CDs as guest species have been explored on account of its potential applications in photoelectrochemical (PEC) water splitting performance. Our synthetic strategy to incorporate well-defined nitrogen-doped carbon dots (N-CDs) array onto zeolitic imidazolate framework-8 (ZIF-8) anchored on ZnO 1D nanostructures allows a facile unification of different components which subsequently plays a decisive role in improving the material's PEC water splitting performance. Simple extension of such strategies is expected to offer significant advantages for the preparation of CDs-based heterostructures for photo(electro)catalytic and other related applications.

Introduction

The demand for alternative clean and sustainable energy storage system has intensified the research on photoelectrochemical water splitting using semiconductor materials as efficient catalysts, primarily for the generation of hydrogen.[1] Among many semiconductor candidates, ZnO is one of the most attractive materials for water splitting reactions due to non-toxicity, low cost, and high electronic conductivity.[2-4] However, there are still significant hurdles that need to be overcome for the effective utilization of ZnO. For instance, the wide band gap (~3.37 eV) of ZnO primarily allows harvesting photons, which are in the UV light region (about 4 % in the solar spectrum).[5,6] Considerable efforts have been reported to reduce the band-gap of ZnO so that the majority of the solar spectrum can be utilized and among them, various carbon or nitrogen doped ZnO lattice are worth-mentioning.[7] Despite such advances, the efficient utilization of solar spectrum without compromising the efficacy of PEC processes still remains a challenge and thus, approaches such as combining more than one component with semiconductor materials (e.g., ZnO) for effective light harvesting and charge-transport are becoming increasingly important. Among such long list of potential components, which can be utilized to improve the efficiency of PEC water splitting, carbon dot photosensitizer (as a new class of carbon nanomaterials) has shown promises because of synergistic effect, when combined with a semiconductor.[8,9] However, the non-homogeneous anchoring and weak bonding between carbonaceous materials and semiconductor materials limit overall efficiency of the process.[10] Though in-situ doping and post-treatment method have been considered as viable alternative approaches, the results show random distribution along the profile from the shell to core and hence require further improvement. Another class of materials, which are also gaining significant attention in this field, is Metal Organic Frameworks (MOFs) due to their tunable porosity, remarkable design flexibility, and high

surface area.[11] Despite the encouraging results from recently reported about MOF-based catalysts for PEC water splitting, the growth of MOFs to the bare surface still remains an area of concern.[12] The current work focuses on the development of a hybrid system combining the three components, namely ZnO nanostructures, Zn-based MOF host and nitrogen-doped CDs (N-CDs) guest to overcome the respective challenges related to the individual components in PEC water splitting. In the present work, our 1D ZnO nanostructure acts as a vertically standing array template and initially hosts Zn^{2+} ions for the formation of ZIF-8 MOF, grown onto them.[13] The ZIF-8 modified ZnO nanostructures are further decorated with N-CDs and the combined heterostructures show significant improvement in PEC water splitting performance when compared to bare ZnO 1D nanostructure.

Results and Discussion

Three types of electrodes were prepared for this study. The ZnO nanotubes directly grown on fluorine doped SnO_2 substrate (Scheme 1a) were prepared by hydrothermal method and subsequent selective etching strategy.[14] The vertically aligned ZnO nanotubes with ZIF-8 (Scheme 1b) and ZnO nanotubes with N-CDs embedded ZIF-8 (Scheme 1c) were synthesized by solvothermal method.[15] Figure 1 represents the scanning electron microscope (SEM) images of ZnO nanotube, ZnO nanotube with ZIF-8, and ZnO nanotube with N-CDs embedded ZIF-8. SEM images (Figures 1a and 1d) show that vertically well aligned ZnO hexagonal nanotubes with outer diameter ranging from 170 to 280 nm and inner diameter between 90 and 140 nm. The coating of ZIF-8 (obtained via solvothermal method) allows the formation of core-shell ZnO@polygon shaped ZIF-8 nanoarrays with high degree of homogeneity (Figures 1b and 1e). The ZnO nanotubes with N-CDs embedded ZIF-8 (~2 μm in thickness and ~320 nm diameter) was simply obtained by adding N-CDs into ZIF-8

precursor solution (Figures 1c, 1d, and S1). The transmission electron microscopy (TEM) images and the corresponding energy dispersive X-ray spectroscopy (EDX) based elemental mapping of ZnO nanotubes with N-CDs embedded ZIF-8 revealed that N-CDs were homogeneously distributed on 1D ZnO nanostructures (Figure 2a-e). The signals corresponding to Zn, O, N, and C elements are uniformly observed over the whole region of 1D nanostructures whereas the high-resolution TEM image of the nanotube edge provides more clear evidence of N-CDs with 0.21 nm of lattice spacing in ZIF-8 (Figure 2f). ZnO nanotubes exhibit a lattice fringe d = 2.6 Å that is assigned to the distance between two (0001) planes of hexagonal wurtzite ZnO nanotube (inset of Figure 2f). Figure S2 represents a strong contrast in the degree of brightness, with dark shell and lighter core, confirming its tubular structure. The metastable (0001) plane of ZnO nanorods with more defects at core has a higher surface energy than the lateral planes, which leads to the preferential etching of the core part of nanorods in the ammonia etching solution, leading to ZnO nanotubes.[16]

Figure 3a shows the current-potential curves of the photoelectrodes under AM 1.5 G (100 mW cm^{-2}) illumination in 0.5 M Na_2SO_4 electrolyte. Most of the photoelectrodes (except ZnO nanotubes with N-CDs embedded ZIF-8) exhibit a photocurrent onset potential at ~0.5 V vs. Ag/AgCl reference electrode that is typical of ZnO. The photocurrent onset of ZnO nanotubes with N-CDs embedded ZIF-8 shows ~ 100 mV cathodic shift compared to others. The photocurrent density of ZnO nanotube arrays with N-CDs embedded ZIF-8 increases dramatically in a potential range from – 0.6 to 0.5 V *vs.* Ag/AgCl as compared the values corresponding to different ZnO nanostructure photoanode, confirming the utility of N-CDs embedded ZIF-8 as photosensitizer with hard contact on ZnO. In this process, the photoelectrode provides more photo-generated electrons and holes because the N-CDs embedded ZIF-8 increase light absorption window of the ZnO nanotube electrode (*vide*

infra).[17] Therefore, the N-CDs embedded ZIF on ZnO nanotubes can not only supply facile electron pathway because of their ordered structure but can also increase the light harvest range and facilitate the separation of electron-hole pairs.[16,18] Figure 3b shows the similar relative trend of transient photo-response measurements. ZnO nanotube arrays with N-CDs embedded ZIF-8 show significantly improved photocurrent density (133% at 0.23 V vs. Ag/AgCl) compared to pristine ZnO nanorods. The Electrochemical Impedance Spectroscopy (EIS) results in Figure 3c exhibit the charge transfer resistance (R_{ct}) in the low frequency zone, which is in accordance with the photocurrent responses. For further quantification of the enhanced PEC performance, incident-photon-to current-conversion efficiency (IPCE) was measured to study the photoresponses of ZnO nanorods, ZnO nanotubes, ZnO nanotubes with ZIF-8, and ZnO nanotubes with N-CDs embedded ZIF-8 (Figure 3d). The IPCE can be expressed as[19]

$$\mathrm{IPCE} = (1240 \times I)/(\lambda \times J_{\mathrm{light}})$$

where I is the photocurrent density, λ the incident light wavelength, and J_{light} the measured irradiance. Pristine ZnO nanorods, ZnO nanotubes, and ZnO nanotubes with ZIF-8 showed strong photoresponse in the UV region and little photoresponse between 400 and 460 nm. ZnO nanotubes with N-CDs embedded ZIF-8 show the strongest photoresponse in the near-UV region along with substantial photoactivity in the visible light region from 520 to 620 nm. The crystal structure of synthesized ZnO nanotube with N-CDs embedded ZIF-8 was confirmed by Powder X-ray diffraction (PXRD) in Figure 4a. The reflection peak located at 34.43^{o} was attributed to a (002) plane, corresponding to [0001] direction growth of ZnO nanotubes, which agrees well with HRTEM results.[20] Additional peaks at 7^{o}, 13^{o}, 16^{o}, and 18^{o}, could be assigned to (011), (1112), (113), and (222) planes of ZIF-8. However, no XRD peaks about N-CDs were observed in ZnO nanotubes with N-CDs embedded ZIF-8 due to the

possible overlap of weak peaks with strong peaks.[21] In addition, the powder XRD patterns (Figure 4c) identified the diffraction peaks at 7^o, 10^o, 13^o, 15^o, 16^o, and 18^o representing the reflections of (011), (002), (112), (022), (113), and (222) planes from the sodalite ZIF-8 respectively.[22] Ultraviolet-Visible absorption spectroscopies (UV-Vis) of the obtained ZnO nanotubes, ZnO nanotubes with ZIF-8, and ZnO nanotubes with N-CDs embedded ZIF-8 are shown in Figure 4b. All the absorptions occurred in the UV light region below 400 nm. Further observation indicates that the optical absorption edge of ZnO nanotubes with N-CDs embedded ZIF-8 showed significant red shift to the visible light region with an increased absorption profile after 380 nm.[23] As shown in the insets of Figure 4b, pristine ZnO nanotubes and ZnO nanotubes with ZIF-8 are white, whereas, ZnO nanotubes with N-CDs embedded ZIF-8 looked brown due to its optical absorption ability in visible light region. The emission color of ZnO nanotubes with N-CDs embedded ZIF-8 photoanode and N-CDs dissolved in ethanol revealed in Figure 4d. Under UV light illumination, the photoanode and N-CDs in the solution exhibited light brown and light greenish-yellow bright emission color, respectively.

Further, we simulated adsorption of carbon dots on Zn nanotubes using model system: we used density functional theory (DFT) for description of coronene (diameter ca. 1nm) or N-doped coronene adsorbed on wurtzite ZnO(10-10) surface. The optimized ZnO structures embody (0001) interlayer distance of 2.60 Å in line with abovementioned experimental value (see also inset of Figure 2f). The optimized model CD structures are physisorbed without covalent bonds (with typical vdW distances 2.6 – 3 Å to surface) and are shown in Figure 5a and b. We also calculated electronic and optical properties of the model systems. The density of states (Figure 5c) gives decreased band gap value when we add coronene or N-doped coronene (with two pyridinic nitrogen atoms; denoted as CorN2pyr) on the surface of ZnO:

2.93 eV for ZnO surface, 1.68 eV for ZnO + Cor and 1.96 eV for ZnO + CorN2pyr. However, since Fermi level alignment is different for these cases, nitrogen doping in carbon dots causes significantly red-shifted absorption (as shown in Figure 5d). Figure 6a, b, and c show different types of N doping with graphitic N positions (two such atoms denoted as N2gra). Despite that electronic band gaps are similar, 2.11 eV (ZnO + CorN2gra), 2.01 eV (ZnO + CorN4gra) and 1.97 eV (ZnO + CorN4graN2pyr), the Fermi level alignment is very different with respect to pure ZnO surface or surface with coronene (nonzero DOS is around Fermi level; Figure 6d) and as the result, absorptions are now nonzero also in red and infra-red region (Figure 6e). These findings are in qualitative agreement with our abovementioned experimental results (see also Figure 4b).

Conclusions

In conclusion, we have explored the simple synthesis method of N-CDs embedded ZIF-8 on 1D ZnO nanotubes without any additional surface modification. Both the experimental results and theoretical analysis proved that 1D ZnO nanotubes with homogeneously anchored N-CDs by ZIF-8 showed superior photocurrent density primarily by enhancing the absorption efficiency in the visible region. Our systematic analysis offers a unique electrode design strategy for making similar hybrid catalysts for PEC water splitting and could be expanded to other metal oxide materials such as TiO_2, Fe_2O_3, and Co_3O_4 aiming towards improved performance PEC water splitting.

Experimental section

Preparation of ZnO Nanotube Arrays on FTO Glass: ZnO nanotube arrays were prepared on FTO glass by hydrothermal and selective etching method. A thin ZnO seed layer was spin-coated on FTO glass with an aqueous solution of 20 mM zinc acetate dihydrate at 4000 rpm for 35 s. ZnO nanorod arrays were grown on the seed layer by a hydrothermal method at 85 ^{o}C for 10 h using a solution containing 25 mM zinc nitrate hexahydrate and 25 mM hexamethylenetetramine as precursor chemicals. The synthesized ZnO nanorods were immersed in an aqueous solution consisting of 0.5 wt% ammonia and 0.5 wt% cetyltrimethyl ammonium bromide (CTAB) at room temperature for 4 h for selective etching of the core.

Preparation of N-CDs embedded ZIF-8 on ZnO Nanotube Arrays: Before synthesizing N-CDs embedded ZIF-8 on ZnO nanotubes, ZnO nanotubes were calcined at 500 ^{o}C in the furnace to remove any surfactant on the surface. The synthesized ZnO nanotube arrays were immersed with conducting side facing down in a Teflon-lined stainless-steel autoclave containing 100 mg 2-methylimidazole, 7 mg N-CDs, and 15 mL of methanol medium. After 30 min of sonication, the autoclave was transferred to the oven at 90 ^{o}C and kept there for 24 h. After cooling at room temperature, the N-CDs embedded ZIF-8 on ZnO nanotubes were mildly washed with water and ethanol to remove any unreacted impurities.

Characterization: N-CDs embedded ZIF-8 on ZnO nanotube arrays were characterized using a field emission scanning electron microscope (FESEM, Hitachi S4800, Japan), a field emission transmission electron microscope (FETEM, JEOL 2010F), high-resolution transmission electron microscope (HRTEM, FEI TITAN G260-300), and X-ray diffraction (XRD, PANalytical, Netherlands) using CuK_{α} radiation.

Evaluation of Electrochemical Properties: The photo-electrochemical experiments of N-

CDs embedded ZIF-8 on ZnO nanotubes were measured with a three-electrode configuration with a Gamry Series 300/Potentiostat/Galvanostat/ZRA instrument under simulated AM 1.5G filter (100 mW cm^{-2}) illumination provided by a solar simulator (150 W Xe). N-CDs embedded ZIF-8 on ZnO nanotube electrodes served as a photoanode, an Ag/AgCl (3 M KCl) as the reference electrode, and a platinum foil as the counter electrode and 0.5 M Na_2SO_4 (pH 6.8) aqueous solution as the electrolyte. The solution was bubbled with N_2 for 30 min prior to each measurement.

Theoretical Analysis: We performed electronic structure calculations using a density functional theory (DFT) corrected by an additional Hubbard-like term (DFT+U). We used the Perdew-Burke-Ernzerhof (PBE) generalized gradient approximation (GGA) to DFT with the effective on-site Coulomb interaction parameters U = 20 eV for Zn atoms and U = 4 eV for O atoms (see details in Supplementary Information text and Figure S4). We used a mixed terminated (10-10) wurzite ZnO layer as model surface (see Figure S5) which is expected in ZnO nanostructures.[24] All the DFT calculations were performed using the VASP code[25] with PAW formalism.[26] For surface calculations with adsorbed coronene, 19.50 Å × 20.83 Å computational supercell with 420 atoms (192 Zn, 192 O, 24 C and 12 H) was used together with 2×2×1 k-point grid and the atomic positions were relaxed until the change in forces was less than 10-2 eV/Å. Cut-off energy of 400 eV was applied. The optical absorption spectrum corresponded to the imaginary part of the dielectric function $\varepsilon(\omega)$. A Gaussian broadening of 50 meV and 128 sampling points were used for the dielectric function.

Acknowledgements

The work at Los Alamos National Laboratory was supported by the NNSA's Laboratory Directed Research and Development Program and was performed, in part, at the Center for Integrated Nanotechnologies, an Office of Science User Facility operated for the U.S.

Department of Energy (DOE) Office of Science. Los Alamos National Laboratory, an affirmative action equal opportunity employer, operated by Los Alamos National Security, LLC, for the National Nuclear Security Administration of the U.S. Department of Energy under contract no. DE-AC52-06NA25396. The authors thank Ondrej Tomanec (from the Regional Centre of Advanced Technologies and Materials, Faculty of Science, Palacky University in Olomouc, Czech Republic) for TEM measurement. F.K. acknowledges institutional support from the University of Ostrava (IRP201826). The calculations were performed at IT4 Innovations National Supercomputing Center (LM2015070).

Notes and references

1 Landman, A. *et al.* Photoelectrochemical water splitting in separate oxygen and hydrogen cells. *Nat Mater* **16**, 646-+, doi:10.1038/Nmat4876 (2017).

2 Wang, M. *et al.* N Doping to ZnO Nanorods for Photoelectrochemical Water Splitting under Visible Light: Engineered Impurity Distribution and Terraced Band Structure. *Sci Rep-Uk* **5**, doi:ARTN 12925

10.1038/srep12925 (2015).

3 Janotti, A. & Van de Walle, C. G. Fundamentals of zinc oxide as a semiconductor. *Rep Prog Phys* **72**, doi:Artn 126501

10.1088/0034-4885/72/12/126501 (2009).

4 Yang, X. Y. *et al.* Nitrogen-Doped ZnO Nanowire Arrays for Photoelectrochemical Water Splitting. *Nano Lett* **9**, 2331-2336, doi:10.1021/nl900772q (2009).

5 Han, H. *et al.* alpha-Fe2O3/TiO2 3D hierarchical nanostructures for enhanced photoelectrochemical water splitting. *Nanoscale* **9**, 134-142, doi:10.1039/c6nr06908h (2017).

6 Chen, H. M. *et al.* Quantum Dot Monolayer Sensitized ZnO Nanowire-Array Photoelectrodes: True Efficiency for Water Splitting. *Angew Chem Int Edit* **49**, 5966-5969, doi:10.1002/anie.201001827 (2010).

7 Lin, Y. G. *et al.* Visible-light-driven photocatalytic carbon-doped porous ZnO nanoarchitectures for solar water-splitting. *Nanoscale* **4**, 6515-6519, doi:10.1039/c2nr31800h (2012).

8 Guo, C. X., Dong, Y. Q., Yang, H. B. & Li, C. M. Graphene Quantum Dots as a Green Sensitizer to Functionalize ZnO Nanowire Arrays on F-Doped SnO2 Glass for Enhanced Photoelectrochemical Water Splitting. *Adv Energy Mater* **3**, 997-1003, doi:10.1002/aenm.201300171 (2013).

9 Xie, S. L. *et al.* Enhanced photoactivity and stability of carbon and nitrogen co-treated ZnO nanorod arrays for photoelectrochemical water splitting. *J Mater Chem* **22**, 14272-14275, doi:10.1039/c2jm32605a (2012).

10 Han, H. *et al.* Dominant Factors Governing the Rate Capability of a TiO2 Nanotube Anode for High Power Lithium Ion Batteries. *Acs Nano* **6**, 8308-8315, doi:10.1021/nn303002u (2012).

11 Wang, W., Xu, X. M., Zhou, W. & Shao, Z. P. Recent Progress in Metal-Organic Frameworks for Applications in Electrocatalytic and Photocatalytic Water Splitting. *Adv Sci* **4**, doi:ARTN 1600371

10.1002/advs.201600371 (2017).

12 Fan, L. L. *et al.* Atomically isolated nickel species anchored on graphitized carbon for efficient hydrogen evolution electrocatalysis. *Nat Commun* **7**, doi:ARTN 10667

10.1038/ncomms10667 (2016).

13 Zhan, W. W. *et al.* Semiconductor@Metal-Organic Framework Core-Shell Heterostructures: A Case of ZnO@ZIF-8 Nanorods with Selective Photoelectrochemical Response. *J Am Chem Soc* **135**, 1926-1933, doi:10.1021/ja311085e (2013).

14 She, G. W. *et al.* Controlled synthesis of oriented single-crystal ZnO nanotube arrays on transparent conductive substrates. *Appl Phys Lett* **92**, doi:Artn 053111 10.1063/1.2842386 (2008).

15 Dong, Y. Q. *et al.* Carbon-Based Dots Co-doped with Nitrogen and Sulfur for High Quantum Yield and Excitation-Independent Emission. *Angew Chem Int Edit* **52**, 7800-7804, doi:10.1002/anie.201301114 (2013).

16 Yu, H. D., Zhang, Z. P., Han, M. Y., Hao, X. T. & Zhu, F. R. A general low-temperature route for large-scale fabrication of highly oriented ZnO nanorod/nanotube arrays. *J Am Chem Soc* **127**, 2378-2379, doi:10.1021/ja043121y (2005).

17 Ye, K. H. *et al.* Carbon quantum dots as a visible light sensitizer to significantly increase the solar water splitting performance of bismuth vanadate photoanodes. *Energ Environ Sci* **10**, 772-779, doi:10.1039/c6ee03442j (2017).

18 Han, H. *et al.* Sb-Doped SnO2 Nanorods Underlayer Effect to the alpha-Fe2O3 Nanorods Sheathed with TiO2 for Enhanced Photoelectrochemical Water Splitting. *Small* **14**, doi:ARTN 1703860

10.1002/smll.201703860 (2018).

19 Parkinson, B. On the Efficiency and Stability of Photoelectrochemical Devices. *Accounts Chem Res* **17**, 431-437, doi:DOI 10.1021/ar00108a004 (1984).

20 Guo, L., Ji, Y. L., Xu, H. B., Simon, P. & Wu, Z. Y. Regularly shaped, single-crystalline ZnO nanorods with wurtzite structure. *J Am Chem Soc* **124**, 14864-14865, doi:10.1021/ja027947g (2002).

21 Gu, Z. G. *et al.* MOF-Templated Synthesis of Ultrasmall Photoluminescent Carbon-Nanodot Arrays for Optical Applications. *Angew Chem Int Edit* **56**, 6853-6858, doi:10.1002/anie.201702162 (2017).

22 Park, K. S. *et al.* Exceptional chemical and thermal stability of zeolitic imidazolate frameworks. *P Natl*

Acad Sci USA **103**, 10186-10191, doi:10.1073/pnas.0602439103 (2006).

23 Wang, L. *et al.* Gram-scale synthesis of single-crystalline graphene quantum dots with superior optical properties. *Nat Commun* **5**, doi:ARTN 535710.1038/ncomms6357 (2014).

24 Wang, Z. L. Zinc oxide nanostructures: growth, properties and applications. *J Phys-Condens Mat* 16, R829-R858, doi:Pii S0953-8984(04)58969-5
10.1088/0953-8984/16/25/R01 (2004).

25 Kresse, G. & Furthmuller, J. Efficient iterative schemes for ab initio total-energy calculations using a plane-wave basis set. *Phys Rev B* 54, 11169-11186, doi:DOI 10.1103/PhysRevB.54.11169 (1996).

26 Kresse, G. & Joubert, D. From ultrasoft pseudopotentials to the projector augmented-wave method. *Phys Rev B* 59, 1758-1775, doi:DOI 10.1103/PhysRevB.59.1758 (1999).

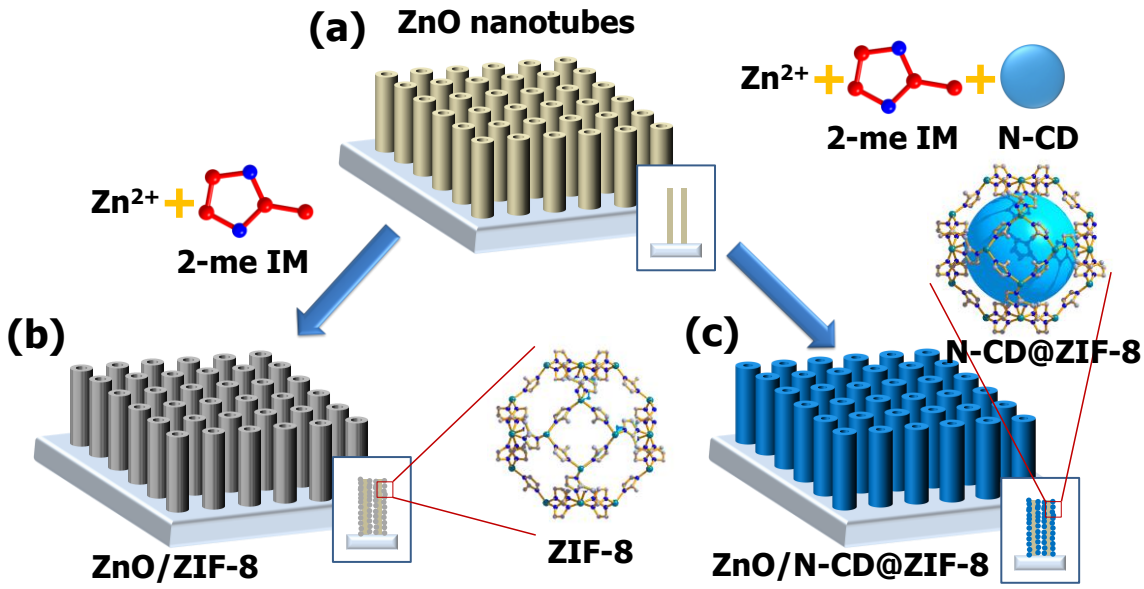

Scheme 1. Schematic illustrations of (a) ZnO nanotubes, (b) ZnO nanotubes with ZIF-8, and (c) ZnO nanotubes with N-CD embedded ZIF-8.

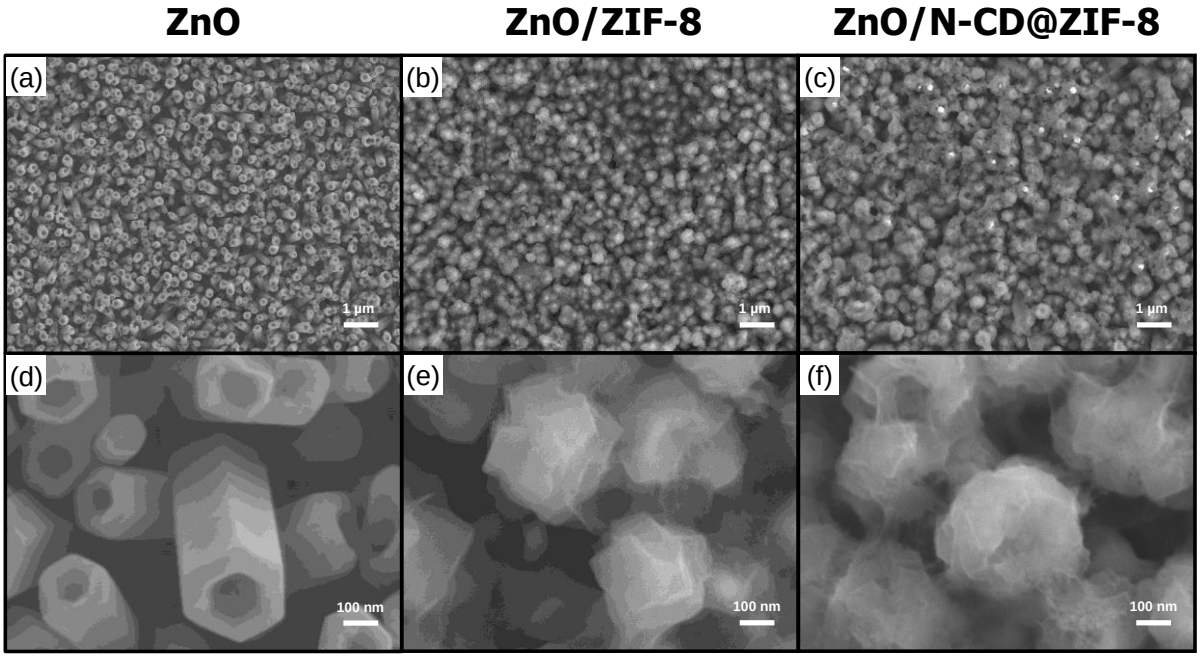

Figure 1. (a,d) Top-view SEM images of ZnO nanotubes, (b, e) ZnO nanotubes with ZIF-8, and (c, f) ZnO nanotubes with N-CD embedded ZIF-8.

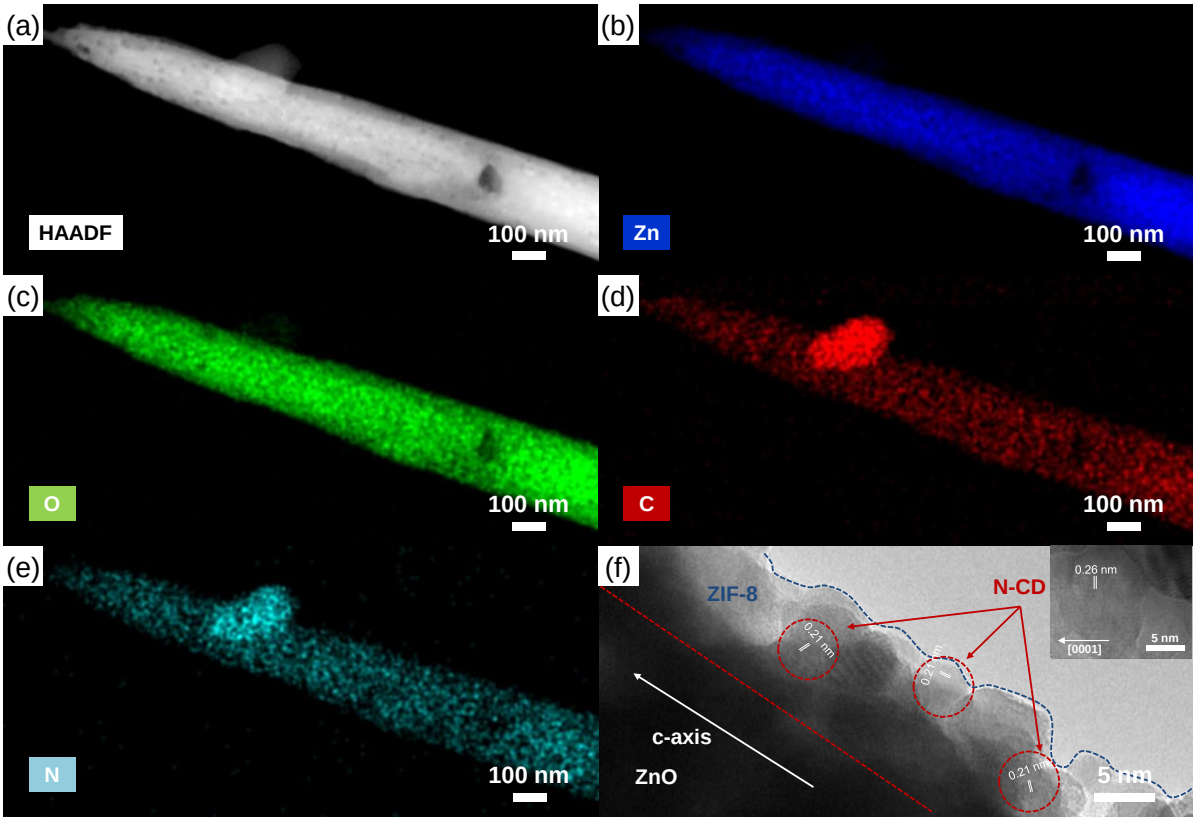

Figure 2. (a-e) HAADF images and (f) HRTEM image of ZnO nanotubes with N-CD embedded ZIF-8.

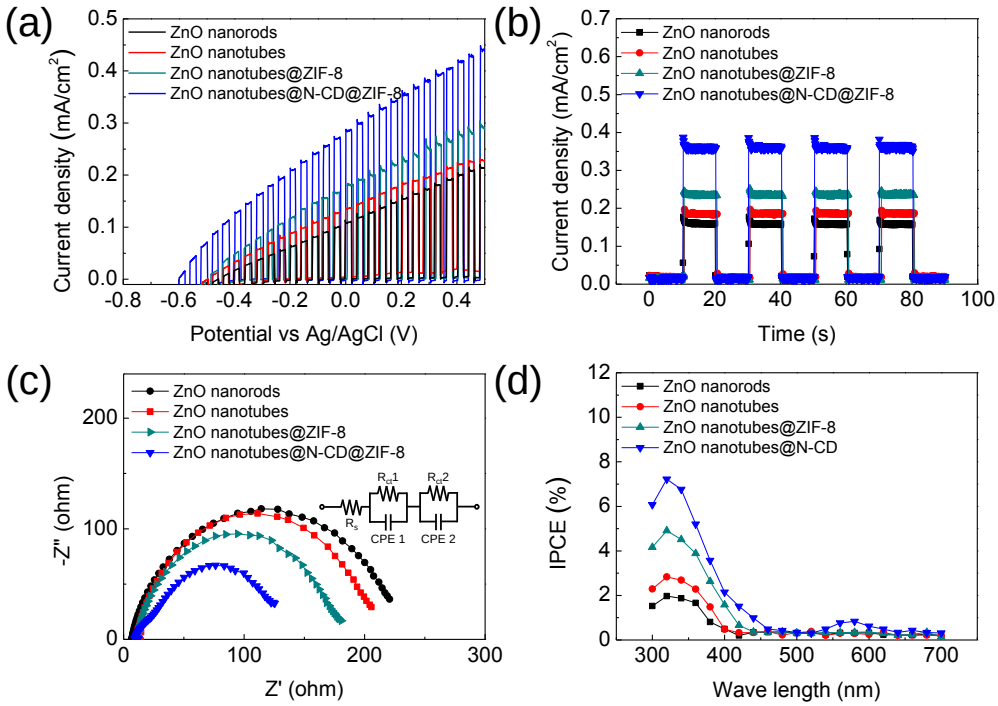

Figure 3. (a) Phototransient characteristics, (b) current-potential characteristics, (c) Nyquist plots of electrochemical impedance measurments (inset: equivalent circuit), and (d) IPCE spectra of ZnO nanorods, ZnO nanotubes, ZnO nanotubes with ZIF-8, and ZnO nanotubes with N-CD embedded ZIF-8.

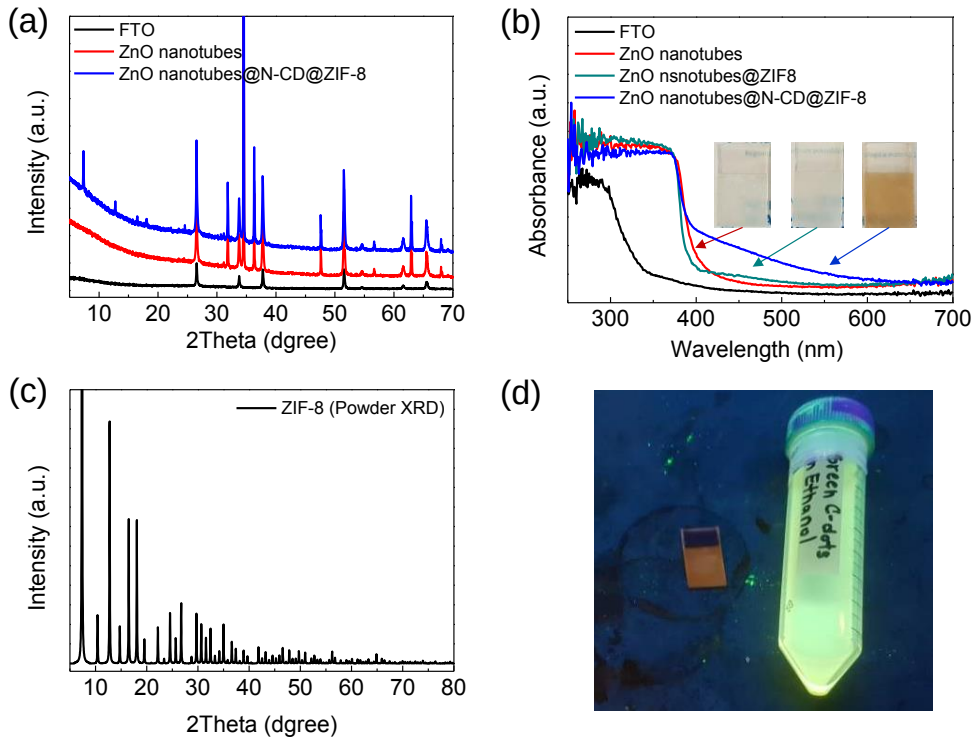

Figure 4. (a) X-ray diffraction pattern and (b) UV-Vis absorption spectra of ZnO nanotubes, ZnO nanotubes with ZIF-8 and ZnO nanotubes with N-CD embedded ZIF-8, (c) X-ray diffraction pattern of ZIF-8. (d) Photograph of N-CDs in Ethanol and ZnO nanotubes with N-CD embedded ZIF-8 under UV light.

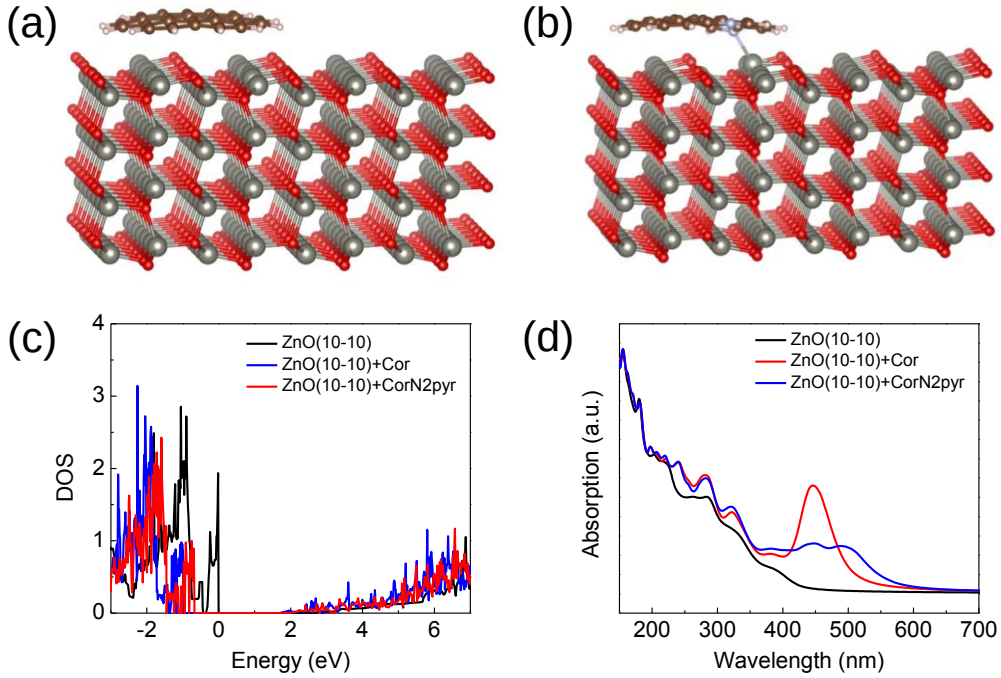

Figure 5. Structure of (a) coronene and (b) N-doped coronene (two pyridinic N atoms) on ZnO(10-10) surface which serve as model for CD on ZnO nanostructure surface. (c) Density of electronic states and (d) optical absorption spectra for ZnO(10-10) surface, ZnO(10-10) with adsorbed coronene (Cor) and ZnO(10-10) with adsorbed N-coronene.

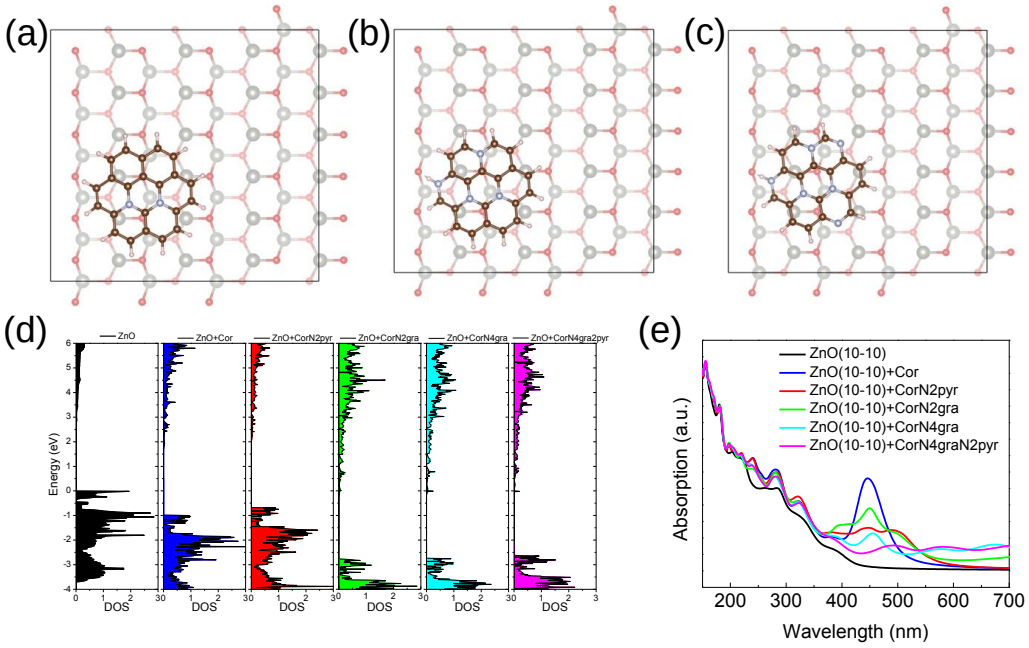

Figure 6. Structure of ZnO surface and adsorbed N-coronene with (a) two graphitic N atoms, (b) four graphitic N atoms and (c) four graphitic and two pyridinic N atoms. (d) Densities of electronic states for various model system. (The Fermi level is set as zero.) (e) Optical absorption spectra for ZnO(10-10) surface and adsorbed N-doped carbon dots.